


RESEARCH ARTICLE

Evaluation of Necrosis Avidity and Potential for Rapid Imaging of Necrotic Myocardium of Radioiodinated Hypocrellins

Qiaomei Jin,^{1,2} Juanzhi Zhao,^{1,2,3} Meng Gao,^{1,2} Yuanbo Feng,^{1,2} Wei Liu,⁴ Zhiqi Yin,⁵ Tiannv Li,⁴ Shaoli Song,⁶ Yicheng Ni,^{1,2,7} Jian Zhang,^{1,2} Dejian Huang,^{1,2} Dongjian Zhang^{1,2} 

¹Affiliated Hospital of Integrated Traditional Chinese and Western Medicine, Nanjing University of Chinese Medicine, Nanjing, 210028, Jiangsu, People's Republic of China

²Laboratories of Translational Medicine, Jiangsu Province Academy of Traditional Chinese Medicine, Nanjing, 210028, Jiangsu, People's Republic of China

³Department of Pharmacy, The Fifth Affiliated Hospital of Sun Yat-sen University, Zhuhai, 519000, Guangdong, People's Republic of China

⁴Departments of Nuclear Medicine, The First Affiliated Hospital of Nanjing Medical University, Nanjing, 210029, Jiangsu, People's Republic of China

⁵Department of Natural Medicinal Chemistry and State Key Laboratory of Natural Medicines, China Pharmaceutical University, Nanjing, 210009, Jiangsu, People's Republic of China

⁶Department of Nuclear Medicine, Renji Hospital, Shanghai Jiaotong University, School of Medicine, Shanghai, 200127, People's Republic of China

⁷Theragnostic Laboratory, KU Leuven, Campus Gasthuisberg, 3000, Leuven, Belgium

Abstract

Purpose: Rapid noninvasive delineation of necrotic myocardium in ischemic regions is very critical for risk stratification and clinical decision-making but still challenging. This study aimed to evaluate the necrosis avidity of radioiodinated hypocrellins and its potential for rapidly imaging necrotic myocardium.

Procedures: The aggregation constants of four natural hypocrellins were analyzed by UV/vis spectroscopy. Then, they were radiolabeled with iodine-131 by iodogen oxidation method. Necrosis avidity of iodine-131-labeled hypocrellins was evaluated in rat models with reperfused liver infarction and muscular necrosis by gamma counting, autoradiography, and histopathology. Their pharmacokinetic properties were examined in normal rats. The potential of iodine-131-labeled hypomycin A ([¹³¹I]HD) for early imaging of necrotic myocardium was explored in rat models with reperfused myocardial infarction. Finally, the possible mechanism of necrosis avidity was investigated by *in vitro* DNA binding and *in vivo* blocking experiments.

Results: The aggregation constants of four hypocrellins were all much smaller than that of hypericin, a most studied necrosis avid agent. The radiochemical purities of the four radiotracers after purification were all greater than 95 %, and more than 90 % of tracers remained intact after incubation in rat serum for 24 h. Among the four tracers, [¹³¹I]HD exhibited the highest necrotic

Qiaomei Jin and Juanzhi Zhao contributed equally to this work.

Correspondence to: Dejian Huang; e-mail: dejianhuang@163.com, Dongjian Zhang; e-mail: zdj168@126.com

to viable tissue uptake ratio and the fastest blood clearance. The necrotic myocardium could be clearly visualized 4 h after injection of [^{131}I]HD by single-photon emission computed tomography/X-ray computed tomography (SPECT/CT). DNA binding studies suggested that HD could bind to DNA through intercalation. Blocking studies demonstrated that uptake of [^{131}I]HD in necrotic muscle could be significantly blocked by excess unlabeled HD and ethidium bromide with 67 and 60 % decline at 6 h after coinjection, respectively.

Conclusions: [^{131}I]HD can be used to rapidly visualize necrotic myocardium. The necrosis avidity mechanism of [^{131}I]HD may be attributed to its binding to the exposed DNA in necrotic tissues.

Key words: Hypocrellins, Necrosis avidity, Self-aggregation, Necrotic myocardium imaging, DNA intercalation

Introduction

Myocardial infarction (MI) remains the predominant cause of morbidity and mortality all over the world. Seasonable myocardial revascularization is currently recognized as the most effective therapeutic method for MI. However, this is not always the case for MI patients. For instance, myocardial revascularization may induce myocardial reperfusion injury [1] and contribute to an extension of infarct size [2] for patients with substantial necrotic myocardium. Therefore, assessment of myocardial viability is essential before revascularization to guide clinical decision-making.

Necrosis avid agents (NAAs) refer to a category of compounds that can selectively accumulate in the necrotic tissues [3], which plays an important role in evaluating myocardial viability and prognosis by noninvasively identifying necrotic myocardium [4]. Several NAAs, including [$^{99\text{m}}\text{Tc}$]pyrophosphate [5], [^{111}In]antimyosin [6], and [$^{99\text{m}}\text{Tc}$]glucarate [7], have been clinically evaluated for visualizing necrotic myocardium. However, they have failed to be used widely in clinical practice in consideration of low target-to-background ratio at early stage or limited imaging time window.

Recently, hypericin (Hyp, Fig. 1a), a potent and prominent NAA, has become a hotspot of research. It had been demonstrated that [^{123}I]Hyp could bind selectively to necrotic myocardium and could be used for imaging of necrotic myocardium [8–10]. However, because of the polyaromatic nature, Hyp is poorly soluble and easily forms supramolecular aggregates in aqueous solution, making it easily accumulate in mononuclear phagocyte system (MPS) such as lung and liver [11–13]. The high uptake in lung and liver not only will increase the radiation burden to normal tissues but also cause interference in the detection of necrotic myocardium, especially in the apex cordis and inferior wall of the left ventricle due to their close proximity to the liver. Therefore, it is desirable to reduce the uptake of NAA in the liver, which should improve the quality for imaging necrotic myocardium.

It has been reported that reducing the conjugated system of aromatic molecules with fused rings can lower their capacity to form self-aggregates [14]. This finding led us to believe that hypocrellins with five conjugated rings might display less degree of aggregation compared with Hyp with

eight conjugated rings. Moreover, splitting of fused rings often could yield new drugs with similar activity in drug research. For example, a series of analgesics with simplified structure and reduced addiction have been successfully developed by splitting the five-membered ring morphine. Similarly, hypocrellins sharing peri-hydroxylated polycyclic quinones with Hyp might still retain necrosis avidity. Based on the above, we speculated that hypocrellins might possess less aggregation capacity and still retained necrosis avidity.

In the present study, we selected four hypocrellin compounds, namely hypocrellin A (HA), hypocrellin B (HB), hypocrellin C (HC), and hypomycin A (HD) (Fig. 1a), and assessed their aggregation capacity by determining their aggregation constants (K_a). After they were labeled with I-131, *in vitro* necrosis avidity was evaluated in necrotic cells and *in vivo* biodistribution was determined in rats with reperfused liver infarction and muscular necrosis. The potential of I-131-labeled HD ([^{131}I]HD) for early imaging of necrotic myocardium was explored in rat models with reperfused MI. Finally, the possible mechanism of necrosis avidity was investigated by *in vitro* DNA binding and *in vivo* blocking experiments.

Materials and Methods

General

Compounds HA, HB, HC, and HD were isolated from the fungus sacs of *Hypocrella bambusae* with purity of over 98 % [15]. Hyp (purity >98 %) was purchased from Purui Technology (Chengdu, China). Sodium iodide ($\text{Na}[^{131}\text{I}]\text{I}$) was supplied by HTA Co., Ltd. (Beijing, China) with radionuclidic purity of greater than 99 % and radioactivity concentration of 740 MBq/ml. All other reagents and solvents were obtained from commercial suppliers and used without further purification. For the *in vitro* cell and *ex vivo* animal studies, radioactivity uptake was measured using a WIZARD² 2470 automated gamma counter (PerkinElmer, Waltham, MA). Kunming mice (male, 25–30 g) and Sprague-Dawley rats (male, 230–250 g) were purchased from Nantong University (Nantong, China) and feed in Experimental Animal Center, Jiangsu Academy of

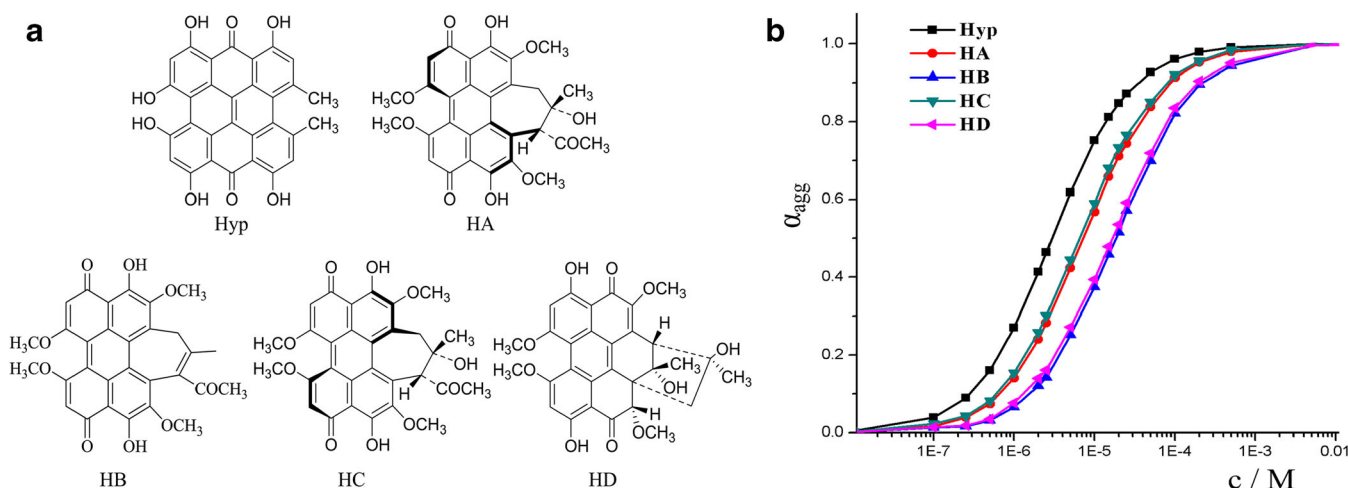


Fig. 1 **a** Chemical structures of hypericin (Hyp), hypocrellin A (HA), hypocrellin B (HB), hypocrellin C (HC), and hypocrellin D (HD). **b** Fraction of aggregated molecules α_{agg} as a function of concentration of Hyp, HA, HB, HC, or HD in 50 % water–DMSO mixture. The lines were acquired by fitting the concentration-dependent UV/Vis data with the isodesmic model.

Traditional Chinese Medicine (Nanjing, China). All animals were given 0.12 % potassium iodide in drinking water from 3 days before the experiment till the end of experiment to protect the thyroid gland from taking up free I-131, and all animal studies were approved by the Institutional Animal Care and Use Committee.

Determination of Aggregation Constants

The self-aggregation constants of HA, HB, HC, HD, and Hyp were measured by a Cary 60 UV–vis spectrophotometer (Agilent Technologies, Santa Clara, CA) according to the method reported by Pietrzak et al. [11]. Measurements were conducted as a function of concentration ranging from 1.0×10^{-8} to 5.0×10^{-4} M at 20 °C and at the wavelength range of 300–700 nm. The isodesmic model was applied for nonlinear regression analysis according to Eq. (1):

$$A(\lambda, C) = [\varepsilon_M(\lambda) - \varepsilon_A(\lambda)] + \frac{2K_a C + 1 - \sqrt{4K_a C + 1}}{2K_a^2 C} + \varepsilon_A(\lambda)C \quad (1)$$

where $A(\lambda, C)$ is absorbance at wavelength λ of the measured samples at total concentration of C in solution; $\varepsilon_M(\lambda)$ and $\varepsilon_A(\lambda)$ are the extinction coefficients for the monomeric and the aggregated compounds, respectively; and K_a is the aggregation constant. The degree of aggregated molecules α_{agg} can be obtained according to Eq. (2):

$$\alpha_{\text{agg}} = 1 - \frac{2K_a c + 1 - \sqrt{4K_a c + 1}}{2K_a^2 c^2} \quad (2)$$

where K_a is the self-aggregation constant and c is the total concentration of the compound.

Radiolabelling and In Vitro Stability

Radioiodination was conducted by adding a DMSO solution of each hypocrellin (0.2 mg/ml) and Na^{131}I solution (4:1, v/v) into a tube coated with 50 μg iodogen. The mixture was incubated at 45 °C for 30 min and then removed from iodogen-coated tube to terminate the reaction. The radiochemical purity was determined by paper chromatography (PC). Whatman No. 1 filter paper was used as stationary phase and 0.1 M hydrochloric acid as developing solvent. The results were presented as percentage of radioactivity of each I-131-labeled hypocrellin relative to the total radioactivity. Purification was performed by a reverse-phase Sep-Pak plus C18 cartridge column (Waters, Milford, MA). After purification, each I-131-labeled hypocrellin was redissolved in a mixture of propylene glycol and polyethylene glycol 400 (1:1, v/v) for cell and animal studies.

For *in vitro* stability assay, 100 μl of each I-131-labeled hypocrellin preparation was added into 900 μl of rat serum and the mixture was incubated for 24 h at 37 °C. The radiochemical stabilities of samples at different incubating time were analyzed by PC as described above.

In Vitro Cell Binding Assays

The human hepatocellular carcinoma cell line HepG2 was obtained from the Shanghai Institute of Cell Biology and cultured in Dulbecco's modified Eagle medium (KeyGen Biotech, Nanjing, China) supplemented with 10 % fetal bovine serum and 1 % (v/v) penicillin/streptomycin at 37 °C in a humidified atmosphere containing 5 % CO_2 .

The HepG2 cells were seeded into a 6-well culture plate at a density of 5×10^5 cells/well and incubated overnight. After being washed with phosphate-buffered saline (PBS), cells were incubated for 1 h at 57 °C to induce necrosis [16]

and at 37 °C as a control. For assessment of the uptake of I-131-labeled hypocrellins in viable and necrotic cells, the cells were transferred into 4-ml Eppendorf tubes and coincubated at 37 °C for 1 h with 0.037 MBq of each I-131-labeled hypocrellin. After centrifugation (12,000 r/min, 10 min), cells were washed twice with cold PBS to remove the unbound tracers. The radioactivity content in cell pellets was measured using a γ counter and expressed as the percentage uptake per 10^8 cells. All experiments were carried out in triplicate.

Pharmacokinetic Studies

Pharmacokinetic studies were performed in normal rats. After intravenous administration of 3.7 MBq of each I-131-labeled hypocrellin ($n=5$), 10 μ l of blood samples was collected *via* a tail incision at 5 min, 10 min, 30 min, 1 h, 2 h, 3 h, 4 h, 5 h, 6 h, 8 h, 12 h, and 24 h post injection (p.i.), respectively. Radioactivity of blood samples was measured with a γ -counter, and corrections were made for physical decay. Radioactivity concentrations in blood samples were calculated and expressed as megabecquerel per liter (MBq/l). The major pharmacokinetic parameters including area under the curve ($AUC_{(0-t)}$, $AUC_{(0-\infty)}$), elimination half-life ($t_{1/2z}$), peak time (T_{max}), clearance (CL_z), peak concentration (C_{max}), and apparent volume of distribution (V_z) were calculated by the noncompartment modeling using Drug and Statistics for Windows 2.0 software.

Animal Models of Necrosis

Rat model with reperfused liver infarction (RLI) and/or muscular necrosis (MN) and rat model with reperfused MI were, respectively, established according to the method described in our previous report [17, 18].

Biodistribution Studies and Blocking Experiment

Biodistribution studies were performed in rats with RLI and MN. After intravenous injection with 3.7 MBq of each I-131-labeled hypocrellin, rats were sacrificed at 6 or 12 h p.i. ($n=5$ per time point). Blocking experiments were performed in rats with MN to verify the specificity of [131 I]HD uptake. For the blocking studies, rats were coinjected with 3.7 MBq of [131 I]HD and excess HD or ethidium bromide (EB) (20 mg/kg) and then sacrificed at 6 h p.i. ($n=5$ per group). The organs of interest were sampled, weighed, and counted for radioactivity by a γ counter. Uptake of the tracers was calculated as percentage of injected dose per gram of tissue (% ID/g).

After γ counting, tissues of normal liver, necrotic liver, and partially necrotic muscle were cut into sections of 30 μ m using a cryostat microtome (Shandon Cryotome FSE; Thermo Fisher Scientific, Waltham, MA) and thaw-

mounted on glass slides. These sections were exposed to a high-performance phosphor screen (PerkinElmer, Waltham, MA) for 4–8 h. Then, the images were acquired by scanning the screen using a Cyclone Plus Phosphor Imager (PerkinElmer). After autoradiography, the sections were stained with hematoxylin and eosin (H&E) according to the routine procedure and digitally photographed.

SPECT/CT Imaging and Postmortem Verification

Rats with MI or sham operation were anesthetized by intraperitoneal injection of 10 % chloral hydrate and placed in supine position. SPECT/CT imaging was performed at 4 h after intravenous administration of 7.4 MBq of [131 I]HD or [131 I]Hyp. The SPECT/CT system (Philips Precedence 6; Philips, Eindhoven, The Netherlands) consisted of a variable angle dual detector equipped with pinhole collimators and a multislice spiral CT component. Images were acquired by the following acquisition parameters: static image matrix size 128 \times 128, continuous acquisition 30 frames \times 25 s/frame, and CT (120 kV, 240 mA). SPECT/CT images were fused using Syntegra software.

After the scan of SPECT/CT, rats were immediately sacrificed and organs of interest were collected, weighed, and counted for radioactivity as described above. The hearts isolated from rats with MI were rinsed with saline and cut into slices of 2 mm in the axial plane. After incubation in 2 % triphenyltetrazolium chloride (TTC) solution at 37 °C for 15 min, the TTC-stained slices were digitally photographed and then cut into 30- μ m slices for autoradiography studies as described above.

DNA Binding Studies

The DNA binding characteristics of HD were studied by measuring changes in UV–visible absorption spectra of fixed concentration of HD with the addition of increasing amounts of DNA. HD was dissolved in 25 % DMSO–Tris–HCl buffer (pH 7.40) mixture. Equal amounts of calf thymus DNA (ct-DNA) were gradually added, and the mixtures incubated at 25 °C for 5 min. The absorption spectra of the mixtures were measured using a Cary 60 UV–vis spectrophotometer (Agilent Technologies, Santa Clara, CA) in the wavelength range of 300–700 nm. The binding constant (K_b) was calculated by the following Eq. (3) [19]:

$$[\text{DNA}]/(\varepsilon_a - \varepsilon_f) = [\text{DNA}]/(\varepsilon_b - \varepsilon_f) + 1/K_b(\varepsilon_b - \varepsilon_f) \quad (3)$$

where [DNA] is the concentration of ct-DNA; the terms ε_a , ε_b , and ε_f correspond to the apparent extinction coefficient and extinction coefficient of free and fully bound compound, respectively, and can be calculated from the Lambert–Beer's law ($\varepsilon = A / [\text{compound}]$). A plot of $[\text{DNA}] / (\varepsilon_a - \varepsilon_f)$ versus

[DNA] gives K_b as the ratio of slope ($1 / (\varepsilon_b - \varepsilon_f)$) to intercept ($1 / K_b (\varepsilon_b - \varepsilon_f)$).

Ethidium bromide (EB) fluorescence quenching experiments were performed to further investigate the binding mode between HD and DNA. The experiment monitored changes in emission intensity of EB bound to DNA as a function of added compound concentration. The ct-DNA was pretreated with EB in a ratio of [DNA]/[EB]=4 at 25 °C for 10 min. After HD was added to the mixture, emission spectra were measured by a Cary Eclipse Fluorescence Spectrophotometer (Agilent Technologies, Santa Clara, CA) in the region of 550–750 nm using an excitation wavelength at 540 nm. The Sterne-Volmer constant (K_{SV}) was calculated according to Eq. (4) [20]:

$$F_0/F = 1 + K_{SV}[Q] \quad (4)$$

where F_0 and F are the fluorescence intensities in the absence and presence of HD and $[Q]$ is the concentration of HD.

Statistical Analysis

Quantitative results were expressed as mean \pm standard deviation (SD). Using the Student's t test, p values less than 0.05 were considered statistically significant.

Results

Determination of Aggregation Constants

The concentration-dependent transitions from monomeric to aggregated hypocrellins and Hyp and the calculated regression lines according to the isodesmic model are presented in Fig. 1b. The aggregation constants of HA, HB, HC, HD, and Hyp were $81,370 \pm 1101$, $32,373 \pm 809$, $90,641 \pm 1047$, $36,151 \pm 1070$, and $199,695 \pm 241$, respectively. Compared to Hyp, aggregation constants of HA, HB, HC, and HD decreased about 59.25, 83.79, 54.61, and 81.90 %, respectively. This indicated that the aggregation capability of hypocrellins was much lower than that of Hyp.

Radiolabeling and In Vitro Stability

The radiolabeling yields of I-131-labeled HA ($[^{131}\text{I}]\text{HA}$), I-131-labeled HB ($[^{131}\text{I}]\text{HB}$), I-131-labeled HC ($[^{131}\text{I}]\text{HC}$), and $[^{131}\text{I}]\text{HD}$ determined by PC were 85.8 ± 2.1 , 74.5 ± 1.8 , 82.3 ± 1.9 , and 97.2 ± 2.0 %, respectively. The radiochemical purities of the tracers after purification were all greater than 95 %. More than 90 % of tracers remained intact after incubation in rat serum for 24 h at 37 °C, indicating that all the tracers had favorable *in vitro* stability.

In Vitro Cell Binding Assays

The uptakes of four iodine-131-labeled hypocrellins in necrotic and viable cells are presented in Table 1. The uptake of $[^{131}\text{I}]\text{HA}$, $[^{131}\text{I}]\text{HB}$, $[^{131}\text{I}]\text{HC}$, and $[^{131}\text{I}]\text{HD}$ in necrotic cells was 3.11, 5.12, 6.39, and 7.37 times as much as that in viable cells, respectively. These results demonstrated that the four I-131-labeled hypocrellins all could selectively bind to necrotic cells.

Pharmacokinetic Studies

The major pharmacokinetic parameters are presented in Table 2. The elimination half-life of $[^{131}\text{I}]\text{HD}$ was 9.05 h, which demonstrated a slightly faster clearance from the blood than $[^{131}\text{I}]\text{HA}$, $[^{131}\text{I}]\text{HB}$, $[^{131}\text{I}]\text{HC}$, and $[^{131}\text{I}]\text{Hyp}$ with elimination half-lives of 10.28, 9.78, 12.17, and 31.20 h [21], respectively.

Biodistribution Studies in Rats with RLI and MN

The biodistribution results of four I-131-labeled hypocrellins in rats with RLI and MN are shown in Table 3. The uptakes of all tracers in necrotic liver and muscle were much higher than those in normal liver and muscle, respectively, at both 6 and 12 h p.i. Among the four tracers, $[^{131}\text{I}]\text{HD}$ demonstrated the highest necrotic-to-normal liver ratios (3.27 and 6.18 for 6 and 12 h p.i., respectively) and necrotic-to-normal muscle ratios (5.56 and 5.49 for 6 and 12 h p.i., respectively). All tracers showed lower uptakes in the examined normal organs at 12 h p.i., but there is only a limited clearance of radioactivity from mostly normal organs from 6 to 12 h p.i.

Autoradiography and Histochemical Staining

Autoradiographs and corresponding H&E staining images of 30- μm liver and muscle slices are presented in Fig. 2. Autoradiography and corresponding H&E staining showed that the uptakes of four I-131-labeled hypocrellins in necrotic liver were much higher than that in normal liver at both studied time points, which was consistent with the

Table 1. Uptake of $[^{131}\text{I}]\text{HA}$, $[^{131}\text{I}]\text{HB}$, $[^{131}\text{I}]\text{HC}$, and $[^{131}\text{I}]\text{HD}$ in HepG2 cells

	% Uptake/ 10^8 cells			
	$[^{131}\text{I}]\text{HA}$	$[^{131}\text{I}]\text{HB}$	$[^{131}\text{I}]\text{HC}$	$[^{131}\text{I}]\text{HD}$
Viable cells	0.47 ± 0.07	0.43 ± 0.06	0.46 ± 0.08	0.43 ± 0.07
Necrotic cells	1.46 ± 0.16	2.20 ± 0.18	2.94 ± 0.25	3.17 ± 0.37
N/V cells	3.11	5.12	6.39	7.37

Data are % uptake/ 10^8 cells and expressed as mean \pm SD
N necrotic, V viable

Table 2. Major pharmacokinetic parameters of [¹³¹I]HA, [¹³¹I]HB, [¹³¹I]HC, and [¹³¹I]HD obtained by noncompartmental modeling after intravenous injection of 3.7 MBq of each tracer in normal rats (*n* = 5)

Parameters	Unit	Pharmacokinetic parameter values			
		¹³¹ I-HA	¹³¹ I-HB	¹³¹ I-HC	¹³¹ I-HD
AUC _(0-t)	MBq/L h	128.99 ± 15.73	205.29 ± 17.99	317.61 ± 15.54	87.94 ± 7.08
AUC _(0-∞)	MBq/L h	157.66 ± 25.47	252.81 ± 38.96	388.25 ± 49.83	101.95 ± 4.49
<i>t</i> _{1/2z}	h	10.28 ± 3.20	9.78 ± 2.40	12.17 ± 3.07	9.05 ± 1.68
<i>T</i> _{max}	h	0.10 ± 0.00	0.08 ± 0.00	0.08 ± 0.00	0.10 ± 0.04
CL _z	L/h/kg	0.10 ± 0.01	0.06 ± 0.01	0.04 ± 0.01	0.15 ± 0.01
<i>C</i> _{max}	MBq/L	35.92 ± 4.32	36.74 ± 1.64	79.03 ± 7.68	26.28 ± 4.93
<i>V</i> _z	L/kg	1.38 ± 0.32	0.82 ± 0.13	0.61 ± 0.08	1.91 ± 0.40

Data are expressed as mean ± SD

results of biodistribution. Moreover, the necrosis avidity of four I-131-labeled hypocrellins was further confirmed by the fact that higher radioactivity uptakes were observed in the necrotic muscle areas than in the viable areas.

SPECT/CT Imaging

Due to the higher necrotic-to-normal tissue ratios and favorable pharmacokinetic properties, [¹³¹I]HD was chosen for SPECT/CT imaging and compared with [¹³¹I]Hyp. Figure 3a displays the representative coronal and transversal SPECT/CT images of rats with MI and control rats with sham operation at 4 h after administration of [¹³¹I]HD or [¹³¹I]Hyp. Obvious hotspot was observed in the heart of a rat with MI while not in the heart of a rat with sham operation after administration of [¹³¹I]HD. In contrast, hotspots were visualized in the hearts of both a rat with MI and a sham-operated rat after administration of [¹³¹I]Hyp. This suggested that [¹³¹I]HD could differentiate necrotic myocardium from viable myocardium at 4 h p.i., while it was not the case for [¹³¹I]Hyp, which was consistent with our previous results [22].

Postmortem Analysis

The radioactivity uptake ratios of organs of interest after SPECT/CT imaging are shown in Fig. 3b. The uptake of [¹³¹I]HD in necrotic myocardium (1.54 ± 0.15 % ID/g) was about 5.58 times that in viable myocardium (0.29 ± 0.05 % ID/g), while uptake of [¹³¹I]Hyp in necrotic myocardium (1.75 ± 0.31 % ID/g) was 3.38 times that in viable myocardium (0.58 ± 0.13 % ID/g). Moreover, [¹³¹I]HD had higher necrotic myocardium-to-lung/blood/liver ratios than [¹³¹I]Hyp (*p* < 0.01). Autoradiographs and corresponding TTC staining images of heart slices from rats with MI are presented in Fig. 3c. The intense signal of autoradiography was localized in necrotic areas as evidenced by TTC staining, which confirmed the preferential accumulation of [¹³¹I]HD and [¹³¹I]Hyp in the necrotic area of myocardium.

DNA Binding Studies

The UV-visible absorption spectra of HD in the absence and presence of increasing amounts of ct-DNA are shown in Fig. 4a. It was reported that hypochromism was generated through an intercalative mode of binding between an aromatic chromophore

Table 3. Biodistribution of [¹³¹I]HA, [¹³¹I]HB, [¹³¹I]HC, and [¹³¹I]HD in rats with reperfused liver infarction and muscular necrosis at 6 and 12 h p.i.

Organ	[¹³¹ I]HA		[¹³¹ I]HB		[¹³¹ I]HC		[¹³¹ I]HD	
	6 h	12 h	6 h	12 h	6 h	12 h	6 h	12 h
Blood	0.65 ± 0.07	0.38 ± 0.03	0.85 ± 0.10	0.56 ± 0.08	0.97 ± 0.10	0.72 ± 0.15	0.59 ± 0.02	0.32 ± 0.05
Brain	0.01 ± 0.00	0.01 ± 0.00	0.01 ± 0.00	0.01 ± 0.00	0.04 ± 0.01	0.02 ± 0.00	0.03 ± 0.10	0.01 ± 0.00
Thyroid	0.13 ± 0.02	0.12 ± 0.03	0.19 ± 0.05	0.21 ± 0.02	0.19 ± 0.06	0.18 ± 0.04	0.18 ± 0.03	0.14 ± 0.04
Lung	0.14 ± 0.01	0.10 ± 0.01	0.65 ± 0.12	0.24 ± 0.05	0.57 ± 0.06	0.37 ± 0.06	0.72 ± 0.02	0.52 ± 0.06
Heart	0.05 ± 0.02	0.04 ± 0.01	0.17 ± 0.04	0.05 ± 0.01	0.15 ± 0.04	0.23 ± 0.07	0.32 ± 0.08	0.27 ± 0.03
Spleen	0.30 ± 0.05	0.24 ± 0.02	0.65 ± 0.08	0.17 ± 0.03	0.89 ± 0.14	0.51 ± 0.15	1.02 ± 0.04	0.64 ± 0.07
Stomach	0.43 ± 0.00	0.30 ± 0.01	0.46 ± 0.10	0.46 ± 0.04	0.61 ± 0.16	0.18 ± 0.03	0.22 ± 0.03	0.19 ± 0.03
Pancreas	0.18 ± 0.02	0.10 ± 0.03	0.21 ± 0.06	0.11 ± 0.01	0.27 ± 0.08	0.26 ± 0.04	0.30 ± 0.04	0.24 ± 0.03
Intestine	0.20 ± 0.06	0.13 ± 0.03	0.25 ± 0.04	0.20 ± 0.05	0.33 ± 0.04	0.36 ± 0.05	0.20 ± 0.04	0.19 ± 0.06
Kidney	0.49 ± 0.04	0.46 ± 0.11	0.33 ± 0.10	0.19 ± 0.03	0.49 ± 0.14	0.40 ± 0.05	0.37 ± 0.04	0.25 ± 0.06
Nor. L.	0.38 ± 0.01	0.31 ± 0.04	0.44 ± 0.10	0.36 ± 0.04	0.94 ± 0.15	0.84 ± 0.06	0.55 ± 0.14	0.51 ± 0.10
Nec. L.	0.53 ± 0.10	0.91 ± 0.05	0.85 ± 0.17	1.32 ± 0.19	1.49 ± 0.23	2.36 ± 0.09	1.71 ± 0.14	3.04 ± 0.46
Nor. M.	0.06 ± 0.01	0.05 ± 0.01	0.07 ± 0.01	0.05 ± 0.01	0.09 ± 0.02	0.06 ± 0.01	0.08 ± 0.02	0.06 ± 0.02
Nec. M.	0.26 ± 0.05	0.19 ± 0.03	0.34 ± 0.06	0.25 ± 0.04	0.36 ± 0.08	0.26 ± 0.04	0.43 ± 0.11	0.32 ± 0.10

Data are % ID/g, expressed as mean ± SD (*n* = 5)

Nor. L. normal liver, Nec. L. necrotic liver, Nor. M. normal muscle, Nec. M. necrotic muscle

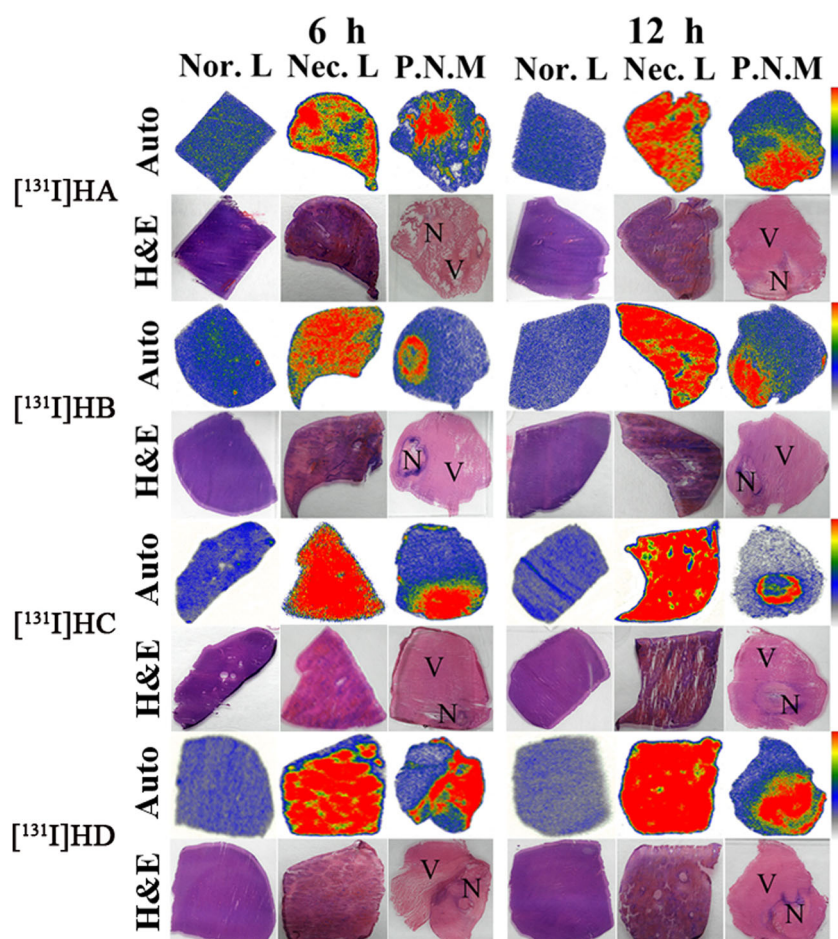


Fig. 2 Autoradiographs (auto) and corresponding H&E staining images of 30- μm liver and muscle slices at 6 and 12 h post injection of $[^{131}\text{I}]\text{HA}$, $[^{131}\text{I}]\text{HB}$, $[^{131}\text{I}]\text{HC}$, and $[^{131}\text{I}]\text{HD}$, respectively. Nor. L normal liver, Nec. L necrotic liver, P. N. M partially necrotic muscle, N necrotic area, V viable area

and the base pairs of DNA [23]. In our present study, with increasing concentrations of ct-DNA, the absorption spectra revealed a “hypochromic” effect, which demonstrated that HD might bind to DNA through an intercalative mode. It was reported that the K_b of a compound binding to DNA by intercalation was usually in the range of 10^4 – 10^6 M^{-1} [24]. The K_b of HD with ct-DNA was found to be $7.36 \times 10^4 \text{ M}^{-1}$, which is within the typical range.

The fluorescence quenching profile of EB-DNA after addition of HD is shown in Fig. 4b. The fluorescence intensity of EB-DNA complex gradually decreased with increasing concentrations of HD, suggesting that EB bound to DNA could be partially replaced by the HD. The K_{SV} value of HD was $5.2 \times 10^4 \text{ M}^{-1}$. This suggested that the interaction mode of HD with DNA should be intercalation, which was consistent with the result of absorption spectroscopy study.

Blocking Experiment

As shown in Fig. 5a, compared with the unblocked group, about 67 and 60 % of the uptake of $[^{131}\text{I}]\text{HD}$ in necrotic

muscle was blocked by coinjection of excess HD and EB, respectively. Uptakes of $[^{131}\text{I}]\text{HD}$ in viable muscles had no significant differences among all groups ($p > 0.05$). The results were further confirmed by autoradiography and H&E staining (Fig. 5b). These results demonstrated that $[^{131}\text{I}]\text{HD}$ should share the same specific target with HD and EB.

Discussion

The present study demonstrated that hypocrellins displayed less aggregation capability compared with hypericin, which may explain the lower uptake of radioiodinated hypocrellins in the MPS organs such as lung and spleen, *etc.* relative to radioiodinated hypericin [21]. Moreover, all four $[^{131}\text{I}]\text{hypocrellins}$ still retained necrosis avidity, and $[^{131}\text{I}]\text{HD}$ could identify necrotic myocardium at 4 h p.i., which was earlier than that of $[^{131}\text{I}]\text{Hyp}$. The necrosis avidity mechanism of $[^{131}\text{I}]\text{HD}$ may be due to its binding to the exposed DNA in necrotic tissues.

Aggregation of Hyp in aqueous solvent is driven largely by π - π interactions and hydrophobic effect of the nearly

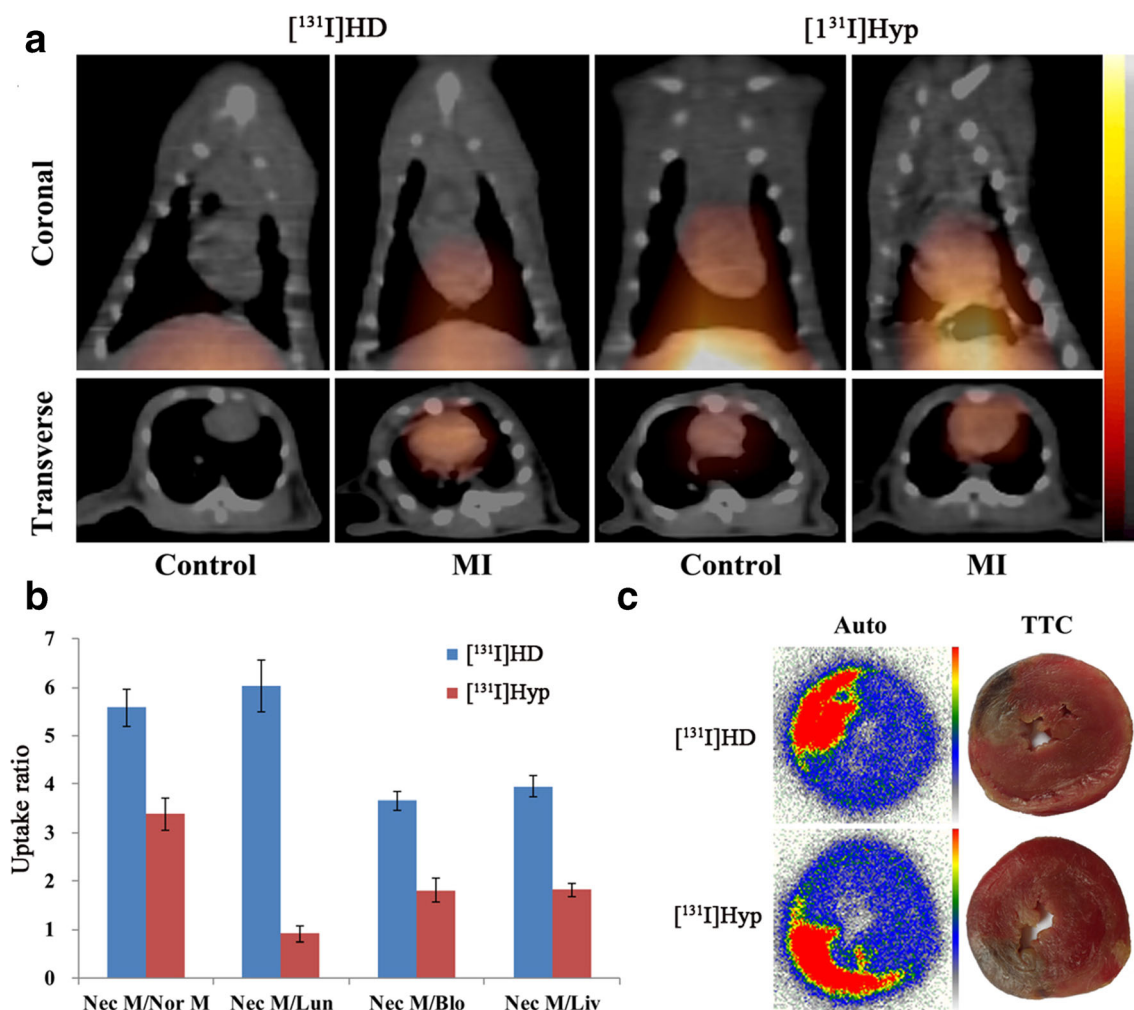


Fig. 3 **a** Coronal and transverse SPECT/CT images in rats with sham operation (control) or myocardial infarction (MI) at 4 h after intravenous injection of $[^{131}\text{I}]\text{HD}$ and $[^{131}\text{I}]\text{Hyp}$, respectively. **b** The uptake ratios of necrotic myocardium-to-normal myocardium/lung/blood/liver for $[^{131}\text{I}]\text{HD}$ and $[^{131}\text{I}]\text{Hyp}$. **c** Autoradiographs (auto) and corresponding TTC staining images of myocardial slices for $[^{131}\text{I}]\text{HD}$ and $[^{131}\text{I}]\text{Hyp}$. Infarcted areas are clearly visible as pale, while viable areas are stained red.

planar π -conjugate aromatic core [25]. Reducing the size of aromatic core or distorting π -conjugated system will weaken π - π stacking interaction between molecules, making the formation of aggregates more difficult [14, 26]. With this in mind, we evaluated the self-aggregation ability and necrosis avidity of four hypocrellins, aiming to find novel NAAs with less aggregation. Our present study demonstrated that hypocrellins displayed less aggregation compared with Hyp and $[^{131}\text{I}]\text{hypocrellins}$ still retained necrosis avidity, which suggested that the strategy to seek for NAAs with less aggregation by splitting polycyclic Hyp was feasible.

The exposed DNA can serve as a molecular target for NAAs [27]. In this study, *in vitro* DNA binding studies indicated that HD could bind to DNA by intercalation. The *in vivo* blocking experiments demonstrated that uptake of $[^{131}\text{I}]\text{HD}$ in necrotic tissues could be significantly blocked by cold HD or EB, a typical DNA intercalator. This suggested that the necrosis avidity mechanism of $[^{131}\text{I}]\text{HD}$

might be due to its binding to the exposed DNA in necrotic tissues.

Some efforts have been made to develop molecular probes targeting exposed DNA. For example, propidium iodide is a routine DNA binding dye used as a marker for necrosis in flow cytometry. However, there appears to be no report on its application in whole-body *in vivo* necrosis imaging. Other DNA binding agents to image necrosis in living organisms included Hoechst-IR and Gd-TO. Hoechst-IR, consisting of a near-infrared IR-786 dye conjugated to Hoechst 33258, could visualize tissue necrosis by fluorescence imaging [28]. Gd-TO could visualize not only acute necrosis but also the clearance of necrotic debris from the infarcted myocardium [29]. However, both of them suffer from potential toxicity problems. Hypocrellins have been used as active components of drug and food additives. Therefore, a necrosis imaging probe based on hypocrellin may have good safety.

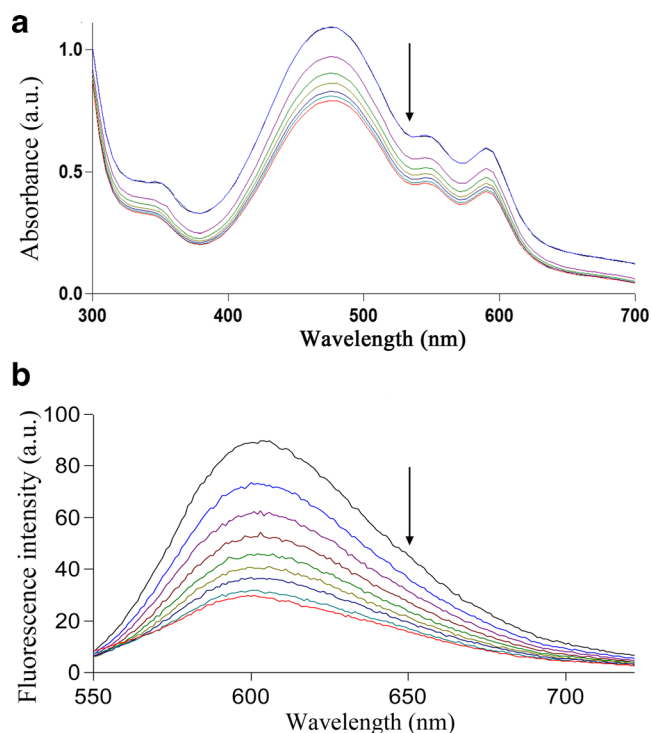


Fig. 4 **a** UV-visible absorption spectra of HD (1.0×10^{-5} M) with the addition of increasing amounts of ct-DNA (0, 0.41, 0.82, 1.23, 1.64, 2.05, 2.46×10^{-5} M). The arrow indicates gradually decreased absorbance upon increasing ct-DNA concentration. **b** Fluorescence emission spectra of EB bound to DNA in the absence and presence of increasing amounts of HD ([DNA] = 5.6×10^{-5} M, [EB] = 1.4×10^{-5} M, [HD] = 0, 0.34, 0.68, 1.02, 1.36, 1.70, 2.04, 2.38, 2.72×10^{-5} M). The arrow shows gradually decreased fluorescence intensity upon increasing amounts of HD.

Although the blocking study results demonstrated a relatively high level of nonspecific accumulation of tracer in the tissues studied, this would not affect the viability of this imaging approach because hotspot was clearly

visualized in the heart of rat with MI while not in the heart of rat with sham operation 4 h after injection of [¹³¹I]HD. *Ex vivo* autoradiography in combination with TTC staining confirmed that the uptake of [¹³¹I]HD was mainly located in infarcted myocardium. This suggested that the “hot spot” in the heart of rat with MI resulted from the specific uptake of [¹³¹I]HD in infarcted myocardium. Therefore, [¹³¹I]HD could be used for imaging MI and held the potential to assess myocardial viability. However, as observed in some of the images in Fig. 2, large necrotic regions within tissue will likely show little or no accumulation of tracer due to the absence of tissue vasculature. In addition, the level of [¹³¹I]HD binding to necrotic tissue will likely be dependent upon tissue perfusion and percentage of necrotic cells within the tissue. Consequently, these factors may limit the assessment of myocardial necrosis and its clinical relevance, which is also currently faced by other necrosis imaging tracers. Therefore, the correlation between the imaging characteristics of myocardial necrosis and *in vitro* histopathological analysis remains to be further evaluated.

[¹²³I]Hyp had been demonstrated to be a potential tracer for the detection of necrotic myocardium [8–10]. However, due to its high blood pool activity, [¹²³I]Hyp could not delineate necrotic myocardium until 9 h p.i. [10]. Although [^{99m}Tc]glucarate can visualize necrotic myocardium at 3 h p.i. [30], it only works within the first 9 h after the onset of MI because of the rapid disintegration of histones which is thought to be the target of [^{99m}Tc]glucarate [31]. Our present study revealed that [¹³¹I]HD could enable visualization of necrotic myocardium at 4 h p.i. in rats with about 24 h of reperfusion after MI. This indicated that [¹³¹I]HD not only had a comparable imaging speed but also had an extended imaging time window compared with [^{99m}Tc]glucarate.

In the present study, I-131 was used for preliminary screening of compounds and imaging studies. However, iodine-131 is rarely used primarily or solely for diagnosis because of its long physical half-life and the burden of its beta radiation on normal tissues. Considering the optimal

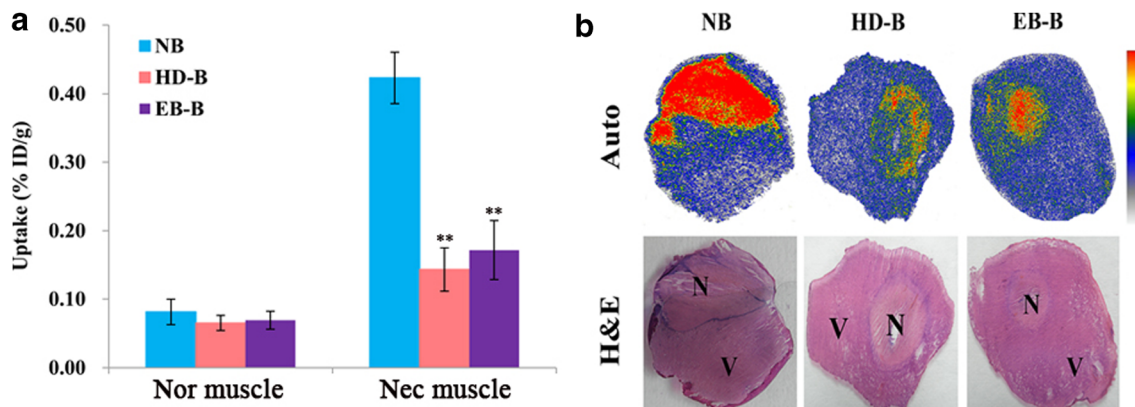


Fig. 5 **a** Uptake of [¹³¹I]HD in unblocked (NB), HD blocked (HD-B), or EB blocked (EB-B) normal (nor) and necrotic (Nec) muscles. The results are presented as % ID/g at 6 h after coinjection. **b** Autoradiographs (auto) and corresponding H&E staining images of 30- μ m muscle slices. N necrotic area, V viable area. ** $p < 0.01$ (uptakes of [¹³¹I]HD in necrotic muscle compared with the unblocked group).

SPECT imaging characteristics of Tc-99m, labeling the HD with Tc-99m would be more appropriate for imaging of necrotic myocardium. Simultaneously, the necrosis avidity mechanism of HD needs to be further clarified.

Conclusion

The present study demonstrated that hypocrellins displayed less self-aggregation and still retained necrosis avidity. [¹³¹I]HD could visualize necrotic myocardium at 4 h p.i., earlier than that of [¹³¹I]Hyp. The necrosis avidity mechanism of [¹³¹I]HD may be due to its binding to the exposed DNA in necrotic tissues.

Acknowledgments. We thank Mr. Yinyan Zhu, Department of Nuclear Medicine, the Affiliated Renji Hospital of Shanghai Jiaotong University School of Medicine, for his technical assistance in SPECT/CT scanning. This study was partially supported by the National Natural Science Foundation of China (Nos. 81473120, 81501536, 81471708).

Compliance with Ethical Standards

Conflict of Interest

The authors declare that they have no conflict of interest.

References

1. Fishbein MC, Y-Rit J, Lando U, Kanmatsuse K, Mercier JC, Ganz W (1980) The relationship of vascular injury and myocardial hemorrhage to necrosis after reperfusion. *Circulation* 62(6):1274–1279. <https://doi.org/10.1161/01.CIR.62.6.1274>
2. White HD, Reynolds HR, Carvalho AC, Pearte CA, Liu L, Martin CE, Knatterud GL, Dzavik V, Kruk M, Steg PG, Cantor WJ, Menon V, Lamas GA, Hochman JS (2012) Reinfarction after percutaneous coronary intervention or medical management using the universal definition in patients with total occlusion after myocardial infarction: results from long-term follow-up of the Occluded Artery Trial (OAT) cohort. *Am Heart J* 163(4):563–571. <https://doi.org/10.1016/j.ahj.2012.01.016>
3. Cona MM, Oyen R, Ni Y (2015) Necrosis avidity of organic compounds: a natural phenomenon with exploitable theragnostic potentials. *Curr Med Chem* 22(15):1829–1849. <https://doi.org/10.2174/0929867322666150227153550>
4. Khaw BA (1999) The current role of infarct avid imaging. *Semin Nucl Med* 29(3):259–270. [https://doi.org/10.1016/S0001-2998\(99\)80014-2](https://doi.org/10.1016/S0001-2998(99)80014-2)
5. Buja LM, Tofe AJ, Kulkarni PV, Mukherjee A, Parkey RW, Francis MD, Bonte FJ, Willerson JT (1977) Sites and mechanisms of localization of technetium-99m phosphorus radiopharmaceuticals in acute myocardial infarcts and other tissues. *J Clin Invest* 60(3):724–740. <https://doi.org/10.1172/JCI108825>
6. Khaw BA, Yasuda T, Gold HK, Leinbach RC, Johns JA, Kanke M, Barlai-Kovach M, Strauss HW, Haber E (1987) Acute myocardial infarct imaging with indium-111-labeled monoclonal antimyosin Fab. *J Nucl Med* 28(11):1671–1678
7. Khaw BA, Nakazawa A, O'Donnell SM et al (1997) Avidity of technetium 99m glucarate for the necrotic myocardium: in vivo and in vitro assessment. *J Nucl Cardiol* 4(4):283–290. [https://doi.org/10.1016/S1071-3581\(97\)90105-7](https://doi.org/10.1016/S1071-3581(97)90105-7)
8. Feng Y, Cona MM, Vunckx K, Li Y, Chen F, Nuyts J, Gheysens O, Zhou L, Xie Y, Oyen R, Ni Y (2013) Detection and quantification of acute reperfused myocardial infarction in rabbits using DISA-SPECT/CT and 3.0 T cardiac MRI. *Int J Cardiol* 168(4):4191–4198. <https://doi.org/10.1016/j.ijcard.2013.07.108>
9. Cona MM, Feng Y, Li Y, Chen F, Vunckx K, Zhou L, van Slambrouck K, Rezaei A, Gheysens O, Nuyts J, Verbruggen A, Oyen R, Ni Y (2013) Comparative study of iodine-123-labeled hypericin and ^{99m}Tc-labeled hexakis [2-methoxy isobutyl isonitrile] in a rabbit model of myocardial infarction. *J Cardiovasc Pharmacol* 62(3):304–311. <https://doi.org/10.1097/FJC.0b013e31829b2c6b>
10. Fonge H, Vunckx K, Wang H, Feng Y, Mortelmans L, Nuyts J, Bormans G, Verbruggen A, Ni Y (2008) Non-invasive detection and quantification of acute myocardial infarction in rabbits using mono-[¹²³I] iodohypericin μ SPECT. *Eur Heart J* 29(2):260–269. <https://doi.org/10.1093/eurheartj/ehm588>
11. Pietrzak M, Maciejczyk M, Szabelski M, Kasperek A, Wiczorek Z (2014) Self-association of hypericin analyzed by light absorption and fluorescence spectroscopy and molecular dynamics simulations. *Chem Phys Lett* 601:39–44. <https://doi.org/10.1016/j.cplett.2014.03.076>
12. Van De Putte M, Roskams T, Bormans G et al (2006) The impact of aggregation on the biodistribution of hypericin. *Int J Oncol* 28:655–660
13. Liu X, Jiang C, Li Y, Liu W, Yao N, Gao M, Ji Y, Huang D, Yin Z, Sun Z, Ni Y, Zhang J (2015) Evaluation of hypericin: effect of aggregation on targeting biodistribution. *J Pharm Sci* 104(1):215–222. <https://doi.org/10.1002/jps.24230>
14. Foster EJ, Jones RB, Laviguer C, Williams VE (2006) Structural factors controlling the self-assembly of columnar liquid crystals. *J Am Chem Soc* 128(26):8569–8574. <https://doi.org/10.1021/ja0613198>
15. Yin Z, Chen Z, Zhang J, Ye W, Zhao S (2013) Chemical constituents of medicinal fungus *Shiraia bambusicola*. *Chin J Chin Mater Med* 38:1008–1013
16. Perek N, Sabido O, Le Jeune N, Prevot N, Vergnon JM, Clotagatide A, Dubois F (2008) Could ^{99m}Tc-glucarate be used to evaluate tumour necrosis? *Eur J Nucl Med Mol Imaging* 35(7):1290–1298. <https://doi.org/10.1007/s00259-007-0689-6>
17. Zhang D, Jiang C, Yang S, Gao M, Huang D, Wang X, Shao H, Feng Y, Sun Z, Ni Y, Zhang J, Yin Z (2016) Effects of skeleton structure on necrosis targeting and clearance properties of radioiodinated dianthrone. *J Drug Target* 24(6):566–577. <https://doi.org/10.3109/1061186X.2015.1113541>
18. Wang Q, Yang S, Jiang C, Li J, Wang C, Chen L, Jin Q, Song S, Feng Y, Ni Y, Zhang J, Yin Z (2016) Discovery of radioiodinated monomeric anthraquinones as a novel class of necrosis avid agents for early imaging of necrotic myocardium. *Sci Rep* 6(1):21341. <https://doi.org/10.1038/srep21341>
19. Barton JK, Danishefsky A, Goldberg J (1984) Tris(phenanthroline) ruthenium(II): stereoselectivity in binding to DNA. *J Am Chem Soc* 106(7):2172–2176. <https://doi.org/10.1021/ja00319a043>
20. Niroomand S, Khorasani-Motlagh M, Noroozifar M, Moodi A (2012) Spectroscopic studies on the binding of holmium-1,10-phenanthroline complex with DNA. *J Photochem Photobiol B* 117:132–139. <https://doi.org/10.1016/j.jphotobiol.2012.09.015>
21. Li J, Zhang J, Yang S, Jiang C, Zhang DJ, Jin Q, Wang Q, Wang C, Ni Y, Yin Z, Song S (2016) Synthesis and preclinical evaluation of radioiodinated hypericin dicarboxylic acid as a necrosis avid agent in rat models of induced hepatic, muscular, and myocardial necroses. *Mol Pharm* 13(1):232–240. <https://doi.org/10.1021/acs.molpharmaceut.5b00686>
22. Duan X, Yin Z, Jiang C, Jin Q, Zhang D, Sun Z, Ye W, Zhang J (2017) Radioiodinated hypericin disulfonic acid sodium salts as a DNA-binding probe for early imaging of necrotic myocardium. *Eur J of Pharm and Biopharm* 117:151–159. <https://doi.org/10.1016/j.ejpb.2017.04.006>
23. Li N, Ma Y, Yang C, Guo L, Yang X (2005) Interaction of anticancer drug mitoxantrone with DNA analyzed by electrochemical and spectroscopic methods. *Biophys Chem* 116(3):199–205. <https://doi.org/10.1016/j.bpc.2005.04.009>
24. Ihmels H, Otto D (2005) Intercalation of organic dye molecules into double-stranded DNA general principles and recent developments. *Top Curr Chem* 258:161–204. <https://doi.org/10.1007/b135804>
25. Bánó G, Staničová J, Jancura D et al (2011) On the diffusion of hypericin in dimethylsulfoxide/water mixtures—the effect of aggregation. *J Phys Chem B* 115(10):2417–2423. <https://doi.org/10.1021/jp109661c>
26. Chen Z, Baumeister U, Tschierske C, Würthner F (2007) Effect of core twisting on self-assembly and optical properties of perylene bisimide dyes in solution and columnar liquid crystalline phases. *Chem Eur J* 13(2):450–465. <https://doi.org/10.1002/chem.200600891>
27. Smith BA, Smith BD (2012) Biomarkers and molecular probes for cell death imaging and targeted therapeutics. *Bioconjug Chem* 23(10):1989–2006. <https://doi.org/10.1021/bc3003309>
28. Dasari M, Lee S, Sy J, Kim D, Lee S, Brown M, Davis M, Murthy N (2010) Hoechst-IR: an imaging agent that detects necrotic tissue in vivo by binding extracellular DNA. *Org Lett* 12(15):3300–3303. <https://doi.org/10.1021/ol100923d>

29. Huang S, Chen HH, Yuan H (2011) Molecular MRI of acute necrosis with a novel DNA-binding gadolinium chelate: kinetics of cell death and clearance in infarcted myocardium. *Circ Cardiovasc Imaging* 4(6):729–737. <https://doi.org/10.1161/CIRCIMAGING.111.966374>
30. Narula J, Petrov A, Pak KY, Lister BC, Khaw BA (1997) Very early noninvasive detection of acute experimental nonreperfused myocardial infarction with ^{99m}Tc -labeled glucarate. *Circulation* 95(6):1577–1584. <https://doi.org/10.1161/01.CIR.95.6.1577>
31. Flotats A, Carrio I (2003) Non-invasive in vivo imaging of myocardial apoptosis and necrosis. *Eur J Nucl Med Mol Imaging* 30(4):615–630. <https://doi.org/10.1007/s00259-003-1136-y>